

Multi-beam scanning electron microscope (MBSEM): Technological evolution, core breakthroughs, and cross-field applications

Wuyang Tan(谭吴洋), Mengni Liu(刘梦妮), Ke Pei(裴科), Chendi Yang(杨辰迪), Jiazhuan Qin(覃家转), Chao Wang(王超), Xuebing Zhao(赵雪冰), and Renchao Che(车仁超)

Citation: Chin. Phys. B, 2026, 35 (**6**): 060705. DOI: 10.1088/1674-1056/ae4c69
http://cpb.iphy.ac.cn; http://iopscience.iop.org/cpb

What follows is a list of articles you may be interested in

Enhancement of thermal conductivity in diamond/Al composites through vacuum-pressure thermal diffusion sintering

Wenxia Zhang(张文霞), Weixia Shen(沈维霞), Chao Fang(房超), Ye Wang(王烨), Yuewen Zhang(张跃文), Liangchao Chen(陈良超), Qianqian Wang(王倩倩), Kenan Li(黎克楠), Biao Wan(万彪), and Zhuangfei Zhang(张壮飞)

Chin. Phys. B, 2025, 34 (**7**): 070703. DOI: 10.1088/1674-1056/adca9e

Combining electron microscopy with atomic-scale calculations—A personal perspective

Sokrates T. Pantelides

Chin. Phys. B, 2024, 33 (**12**): 120704. DOI: 10.1088/1674-1056/ad8ece

Capturing the non-equilibrium state in light—matter—free-electron interactions through ultrafast transmission electron microscopy

Wentao Wang(汪文韬), Shuaishuai Sun(孙帅帅), Jun Li(李俊), Dingguo Zheng(郑丁国), Siyuan Huang(黄思远), Huanfang Tian(田焕芳), Huaixin Yang(杨槐馨), and Jianqi Li(李建奇)

Chin. Phys. B, 2024, 33 (**1**): 010701. DOI: 10.1088/1674-1056/ad0141

Design of a novel correlative reflection electron microscope for *in-situ* real-time chemical analysis

Tian-Long Li(李天龙), Zheng Wei(魏征), and Wei-Shi Wan(万唯实)

Chin. Phys. B, 2021, 30 (**12**): 120702. DOI: 10.1088/1674-1056/ac0522

Design of an ultrafast electron diffractometer with multiple operation modes

Chun-Long Hu(胡春龙), Zhong Wang(王众), Yi-Jie Shi(石义杰), Chang Ye(叶昶), and Wen-Xi Liang(梁文锡)

Chin. Phys. B, 2021, 30 (**9**): 090701. DOI: 10.1088/1674-1056/ac11cd

---

REVIEW

Multi-beam scanning electron microscope (MBSEM): Technological evolution, core breakthroughs, and cross-field applications

Wuyang Tan(谭吴洋)[†], Mengni Liu(刘梦妮)[†], Ke Pei(裴科), Chendi Yang(杨辰迪), Jiazhuan Qin(覃家转), Chao Wang(王超), Xuebing Zhao(赵雪冰), and Renchao Che(车仁超)[‡]

Laboratory of Advanced Materials, Shanghai Key Laboratory of Molecular Catalysis and Innovative Materials, State Key Laboratory of Coatings for Advanced Equipment, College of Smart Materials and Future Energy, Fudan University, Shanghai 200438, *China*

(Received 17 December 2025; revised manuscript received 24 February 2026; accepted manuscript online 3 March 2026)

Multi-beam scanning electron microscope (MBSEM) reconciles the inherent contradiction between "resolution and throughput" of traditional scanning electron microscopes (SEMs) through parallel electron beam manipulation, emerging as a key technology to address the bottlenecks in large-volume, high-resolution imaging and advanced industrial inspection. This article provides a comprehensive overview of MBSEM, covering its evolutionary course of technology, core design fundamentals, and interdisciplinary applications. First, it sorts out the evolutionary process from conceptualization in the early 21st century to commercialization in the 2010s, clarifying the core logic of breaking through the physical limitations of single-beam systems via "multi-beam parallelism". Subsequently, focusing on the core technological chain of "beam generation–optical focusing–signal detection–data processing", it conducts an in-depth analysis of the design concepts, technical characteristics, and applicable scenarios of three mainstream architectures: the single-source single-column, split optical system, and semiconductor-specific multi-beam inspection (MBI). Combined with representative research and product data from teams such as Delft University of Technology, Zeiss, and ASML/HMI, it reveals the differentiated advantages of each architecture in beam uniformity (the relative deviation percentage of the current density and probe size of each sub-beam in the multi-beam array from the central beam, with a smaller deviation value indicating better uniformity) and signal crosstalk (the percentage of the interference signal intensity to the target signal intensity when the detection signal of a single beam in the multi-beam array interferes with the detection channel of adjacent beams) control, and throughput (the percentage of the interference signal intensity to the target signal intensity when the detection signal of a single beam in the multi-beam array interferes with the detection channel of adjacent beams) improvement. Finally, integrating the practical demands of neuroscience connectomics, advanced semiconductor manufacturing processes, and biomedicine, it elaborates on the application breakthroughs of MBSEM in the three-dimensional (3D) reconstruction of large-volume brain tissue, wafer defect screening for 7 nm and smaller nodes, and low-damage imaging of thin biological tissues, and compares its disruptive value relative to traditional technologies (single-beam SEM, optical inspection).Unlike previous reviews, this work systematically integrates both academic prototypes and industrial systems for the first time, providing an in-depth analysis of the differentiated trade-offs among imaging speed, resolution, and sample adaptability across different architectures, offering a systematic reference for MBSEM R & D and interdisciplinary applications.

Keywords: multi-beam scanning electron microscopy (MBSEM), parallel imaging technology, connectomics, advanced semiconductor process inspection, beam control and signal processing

PACS: 07.78.+s, 07.77.Ka, 85.40.–e, 85.85.+j

DOI: 10.1088/1674-1056/ae4c69 **CSTR:** 32038.14.CPB.ae4c69

1. Introduction

Scanning electron microscopy (SEM) has served as a key tool in biomedicine, materials science, and industrial inspection since its commercialization in the 1960s,[1–8] thanks to its nanoscale spatial resolution. However, with the surge in demand for "large-volume and high-resolution" simultaneous imaging in cutting-edge fields, the intrinsic physical limitations of traditional single-beam SEM have become increasingly prominent. In neuroscience, connectomics requires mapping the complete connection atlas of neurons within a millimeter-scale volume (e.g., mouse cerebral cortical column of 400 μm×400 μm×1000 μm). Single-beam SEM imaging with 4-nm pixels and 30-nm section thickness takes over 500 days,[9] while imaging 1 mm^3 of brain tissue even requires 12 years,[10,11], far exceeding the tolerance range of research cycles. In the semiconductor industry, wafer inspection for 7 nm and below nodes requires scanning hundreds of square millimeters per hour. However, constrained by Coulomb interaction (beam blurring caused by increased current) and detector bandwidth limitations (single detector bandwidth is usually

[†]These authors contributed equally to this work.

[‡]Corresponding author. E-mail: rcche@fudan.edu.cn

© 2026 Chinese Physical Society and IOP Publishing Ltd. All rights, including for text and data mining, AI training, and similar technologies, are reserved.

$<$ 20 MHz), the detection mode — SE (secondary electron) — the throughput of single-beam SEM is only 1/100 that of optical inspection,[12], failing to meet the efficiency requirements in mass production scenarios.

To address these challenges, multi-beam SEM (MBSEM) emerged in the early 21st century with its core innovation being "multi-beam parallel scanning" to achieve synergistic "resolution–throughput" enhancement. Theoretically, total imaging throughput is proportional to the number of beams, while distributing total current across multiple beams reduces single-beam current density, minimizing Coulomb interaction effects on resolution.[13,14] MBSEM technology accelerated its development in the 2010s: Delft University of Technology unveiled a 196-beam (14×14 array) MBSEM prototype in 2010, featuring a ZrO/W Schottky source and microfabricated aperture lens array (ALA). This breakthrough achieved a 1 nm probe size with 31 pA single-beam current, landing energy: 15 keV, validating the feasibility of hundred-level beam parallelism;[15,16] in 2015, Zeiss introduced the commercial MultiSEM 505 (61 beams) with hexagonal ALA arrangement and magnetic beam separator design. This reduced mouse cortical column imaging time to 1/60 of that of a single-beam SEM,[17] pixel size: 4 nm, sample type: mouse brain cortical tissue, detection mode: SE, advancing MBSEM from laboratory research to practical biological imaging applications; ASML's HMI division targeted semiconductor inspection requirements with the 2020 release of a 9-beam MBI system (eScan1000 series), boosting wafer defect detection throughput by 4–6 times, sample type: 7 nm node silicon wafer, detection mode: VC (voltage contrast). A 25-beam system is projected to achieve 10–13 times improvement, establishing MBSEM as essential equipment for 7 nm and smaller node inspection.[18]

Today, MBSEM has established a technical system covering "basic research–industrial application". Its technological evolution not only reflects the interdisciplinary integration of electron optics, signal detection, and data processing, but also promotes the transformation of fields such as neuroscience, semiconductors, and biomedicine from "local sampling analysis" to "full-scale high-throughput research". Based on representative literature and product progress in the MBSEM field in recent years, this paper systematically sorts out its technical principles, core breakthroughs, and application scenarios, analyzes current challenges and looks forward to future directions, so as to provide references for the further development and application of this technology.[14]

2. Core technical principles and architectural innovations of MBSEM

The essence of MBSEM is high-throughput imaging realized through "parallel electron beam manipulation." Its technological development has consistently revolved around three core challenges: "how to efficiently generate uniform multi-beam arrays, prevent crosstalk between multiple beams, and synchronously process parallel data." Different research teams, driven by application requirements, have developed three mainstream architectures: single-source single-column, split-optical systems, and semiconductor-specific MBI. These architectures complement one another in design philosophy, technical characteristics, and applicable scenarios, collectively driving the maturation of MBSEM technology.

2.1. Technology evolution path: from proof of concept to commercial deployment

The concept of MBSEM can be traced back to the early 21st century, when research focused on "how to achieve parallel generation and focusing of multiple beams." Early explorations primarily relied on single-source splitting techniques, using microfabricated aperture arrays to divide the wide-angle beam from a single electron source into multiple sub-beams. In 2008, the Kruit team at Delft University of Technology proposed a multi-beam generation scheme based on Schottky sources and an aperture lens array (ALA). By adjusting the ALA electrode voltage to correct field curvature aberrations, they reduced off-axis beam aberrations by 30%, laying the foundation for subsequent hundred-beam systems. In 2010, the team unveiled a 196-beam MBSEM prototype. Utilizing a 14×14 ALA (aperture diameter 18 μm, pitch 25 μm) with an immersion objective, it achieved a 1-nm probe size and 31-pA single-beam current, with beam current uniformity fluctuations $<$ 5%. This demonstrated the feasibility of parallel imaging with hundreds of beams for the first time. The period from 2010 to 2020 marked a pivotal phase in the commercialization of MBSEM, with core breakthroughs achieved in "signal separation and system integration." Addressing the demand for large-volume biological imaging, the Zeiss team introduced the MultiSEM 505 (61 beams) in 2015. Featuring a hexagonal ALA arrangement (80% fill factor) and a magnetic beam separator design, it deflects SE signals 90° to the array detector, achieving crosstalk $<$ 5% and a resolution difference between edge and center beams $<$ 3%. This system reduced imaging time for a mouse cortical column (400 μm×400 μm×1000 μm) from 505 days with a single beam to 25 days, propelling connectomics research into the era of "large-volume high-efficiency imaging". During the same period, the Hitachi team focused on medium-to-low resolution inspection in semiconductors. They proposed a split optical system architecture that separated the photoelectric (PE) and shot noise (SE) paths using Wien filters. Combined with dual condenser lenses to eliminate image rotation, this achieved 4-beam parallel imaging with a signal separation efficiency of 99%, suitable for defect screening on 22-nm node wafers. After 2020, MBSEM technology evolved toward "high density and high sensitivity," ex-

emplified by ASML/HMI's semiconductor-specific MBI systems. The team's 2020 release of the 9-beam MBI system (eScan1000) employs MEMS technology to independently adjust each beam's astigmatism, achieving beam current uniformity fluctuations $< 2\%$. It integrates a 50-Gbps computing architecture with a high-speed stage (reducing travel time from 90 ms to 10 ms), boosting physical defect detection throughput by 5.7 times. EUV mask verification defect capture rate $> 99\%$, establishing it as the core tool for full-process inspection at 7 nm and below nodes.

2.2. Mainstream architecture comparison: design philosophy and applicable scenarios

2.2.1. Single-source–single-column architecture: balancing compactness and source utilization

Single-source–single-column architecture is built upon the core design principle of "achieving multi-beam parallelism through a single electron source and a shared optical column." Its technical approach involves: a single high-brightness electron source (such as a Schottky source) generates a wide-angle beam, which is split into multiple sub-beams by an ALA. These sub-beams are then focused onto the sample using the same set of electron optical columns (condenser lens, objective lens). SE/TE signals are simultaneously acquired by the built-in detection system. The key advantage of this architecture lies in its high electron source utilization. The unused portion of the Schottky source's wide angular distribution can be reused through multi-beam multiplexing. Its compact size allows integration into conventional SEM vacuum chambers, making it the mainstream choice for biological imaging and general detection. The 196-beam prototype from Delft University of Technology and the Zeiss multi-SEM series are representative examples of this architecture. In core component design, both employ Schottky field emission sources (luminance 5×10^7 A/(m^2·sr·V), energy dispersion 0.5 eV FW50), ensuring the beam maintains a single-beam current of 30 pA–700 pA while sustaining a hundred-level beam; for the ALA design, Delft employs a 14×14 square array. By adjusting the E1/E2 electrode voltage to correct the field curvature, the off-axis beam focal plane aligns with the on-axis plane, reducing the aberration contribution from 1.0 nm to 0.4 nm. Zeiss employs a hexagonal ALA with edge apertures slightly larger than the central aperture, balancing off-axis beam current density and achieving full-field current uniformity fluctuations $< 5\%$. For signal detection, Zeiss employs a magnetic beam splitter to deflect the SE onto an array detector, achieving crosstalk $< 5\%$. Delft University of Technology utilizes a YAG crystal-fiber coupling scheme, yielding an SE conversion efficiency of 21 photons/keV, a detection efficiency of 13%, and crosstalk $< 2\%$. The limitations of this architecture include beam count constrained by ALA size (current maximum 196 beams) and the need for complex aberration correction (e.g., multipole correctors) for off-axis beams. Consequently, it is better suited for large-volume biological imaging (e.g., 3D brain tissue reconstruction) and general material characterization, but struggles to meet semiconductor inspection demands for "high-density beams + real-time defect identification," as illustrated in Fig. 1(a).

2.2.2. Separate optical system architecture: independent optimization of illumination and detection

Unlike the single-source–single-column architecture, the core design philosophy of the split optical system architecture lies in physically separating the illumination path from the detection path, allowing independent optimization of the two subsystems: the illumination subsystem focuses on multi-beam focusing uniformity, while the detection subsystem can be specifically corrected for secondary electron aberrations and crosstalk, thereby achieving higher signal separation purity. The split optical system architecture is designed to address "signal separation stability" requirements, dividing the optical system into a "primary beam illumination subsystem" and an "SE detection subsystem." Wien filters or magnetic deflectors achieve complete separation of the PE and SE paths. The illumination subsystem focuses on multi-beam focusing uniformity, while the detection subsystem independently optimizes SE aberrations and crosstalk (the percentage of the interference signal intensity to the target signal intensity when the detection signal of a single beam in the multi-beam array interferes with the detection channel of adjacent beams). This prevents mutual interference between PE and SE, making it suitable for scenarios demanding high signal purity (e.g., low-resolution inspection in semiconductors). Hitachi's four-beam MBSEM exemplifies this architecture, as shown in Fig. 1(b), with core design breakthroughs in dual-condenser illumination and SE aberration suppression. The illumination subsystem employs MEMS-fabricated 4-beam ALA. Dual condenser lenses eliminate image rotation, ensuring uniform multi-beam incidence angles (perpendicular to the sample surface). Beam spacing is 110 μm, single-beam FOV is 250 μm, and focusing deviation is $< 5\%$. The SE detection subsystem compresses aberrations via accelerated electric fields (3 keV–9 keV). When SE energy increases from 3 keV to 9 keV, aberrations decrease to 1/4, and SE separation efficiency rises from 20% to 99%. Simultaneously, a "scan-compensating deflector" was introduced to synchronously compensate for SE positional shifts caused by PE scanning, preventing signal spillage to adjacent detectors with crosstalk (the percentage of the interference signal intensity to the target signal intensity when the detection signal of a single beam in the multi-beam array interferes with the detection channel of adjacent beams) controlled below $< 3\%$. The advantage of this architecture lies in its superior signal separation stability compared to single-source–single-column configurations. However, it operates

with fewer beams (currently up to 4 beams), resulting in limited throughput enhancement. It is primarily used for defect screening on semiconductor 22-nm node wafers (e.g., particle detection, linewidth deviation measurement) and struggles to meet the high-throughput demands of 7 nm and below nodes. Figure 1(c) illustrates the modeling of a multi-beam source (MBS) coupled with an accelerator lens using electron–optics design software (EOD). Its core function is to visualize the structural relationship between the two components, beam transmission paths, and imaging effects. This figure provides intuitive validation of the coupling feasibility between MBS and accelerator lenses: it demonstrates that after generation from the MBS, the multiple beams can be stably transmitted through the accelerator lens while maintaining their array configuration, without significant divergence or deflection. It also clarifies the imaging logic: the accelerator lens does not directly focus the MBS beams onto a physical plane but instead forms a virtual image through refraction. Figure 1(d) schematically illustrates "common intersection point diffusion" caused by the spherical aberration of the accelerator lens.[19] Its core function is to visually demonstrate how spherical aberration in the accelerator lens disrupts the "common intersection point" (the intended convergence location for all beams) within the multi-beam system, particularly highlighting the impact on outer-layer beams.

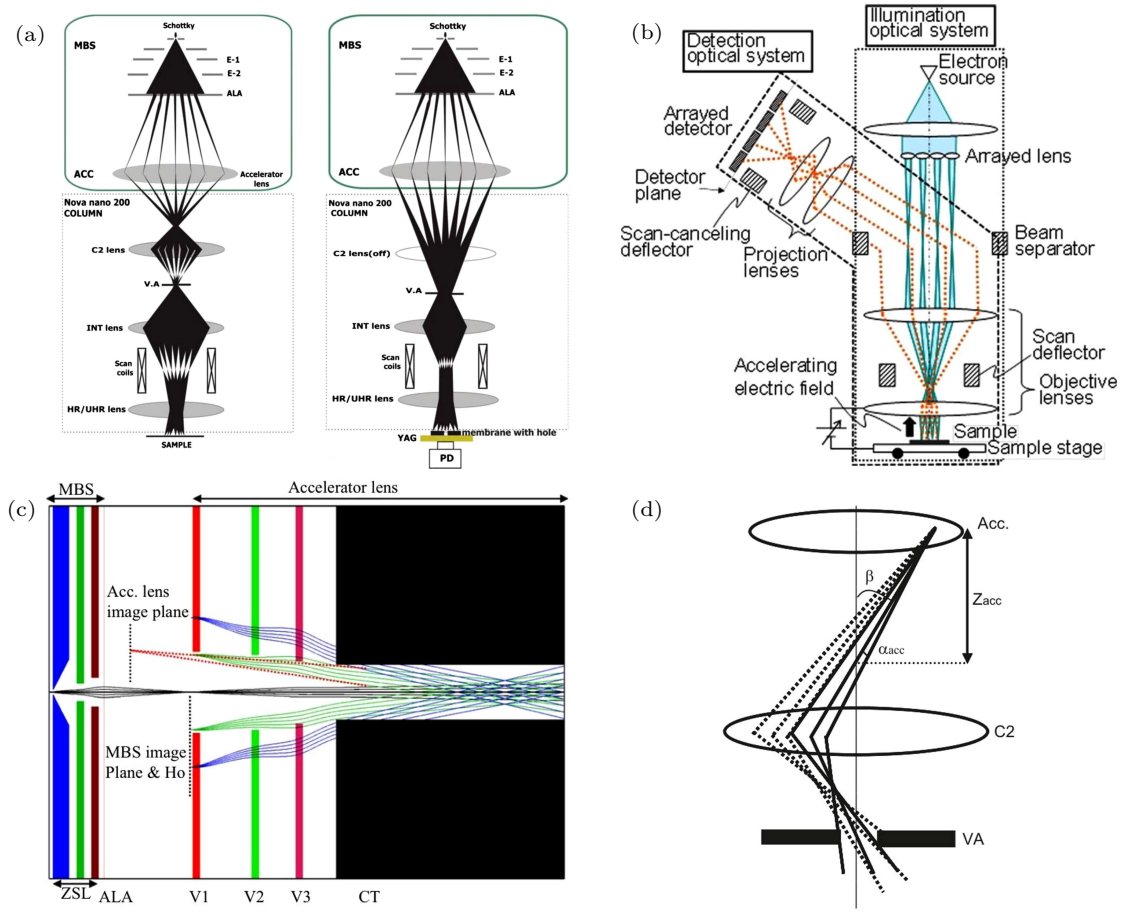


Fig. 1. Schematic diagrams of MBSEM optical system architectures. (a) Core electron optical system schematic diagram of the single-source single-column architecture,[22] reproduced with permission from Ref. [22]: The left diagram illustrates the complete working principle, embodying the core logic of "multi-beam generation–transmission–imaging/measurement"; the right diagram shows a dedicated configuration for single-beam size measurement at fixed magnification. This architecture is characterized by high electron source utilization and compact design, making it suitable for large-volume biological imaging; (b) schematic diagram of Hitachi's novel optical system for multi-beam scanning electron microscopy (SEM),[20] reproduced with permission from Ref. [20]: physical separation of illumination and detection paths is achieved through a Wien filter, allowing independent optimization of the two subsystems with signal separation purity $> 99\%$, suitable for defect screening at 22-nm semiconductor nodes; (c) schematic diagram of the multi-beam source (MBS) coupled with accelerator lens configuration modeled using electron optical design (EOD) software,[19] reproduced with permission from Ref. [19]: Visual validation that multiple beams can stably transmit through the accelerator lens while maintaining array configuration after generation from the multi-beam source, providing theoretical basis for optical system design. (d) Schematic illustrating "co-intersection diffusion" caused by spherical aberration in the accelerator lens,[19] reproduced with permission from Ref. [19]: Visual demonstration of how spherical aberration disrupts the ideal common intersection point in multi-beam systems, particularly highlighting the displacement of outer beams, explaining the necessity of off-axis aberration correction.

2.2.3. Semiconductor-specific MBI architecture: synergy of high throughput and high sensitivity

The semiconductor-specific MBI architecture addresses defect detection requirements for 7 nm and below nodes through an integrated design combining "high-density beam arrays + high-speed signal processing + precision stages." Its core objective is to balance "defect capture rate versus throughput," with the technical approach focused on "enhanc-

ing beam uniformity, reducing inspection time, and enabling real-time defect identification." ASML/HMI's eScan1000 series exemplifies this architecture, showcasing three key technical features: First, a high-density uniform beam array employing $3 \times 3/5 \times 5$ configurations with a minimum single-beam pixel size of 2 nm. MEMS technology independently adjusts astigmatism for each beam, achieving beam current uniformity fluctuations $< 2\%$ to meet 7-nm node defect detection sensitivity requirements.[12] Second, high-speed signal processing integrates a 50-Gbps distributed computing architecture, enabling real-time defect recognition (e.g., die-to-database comparison) and achieving data compression ratios exceeding 10^6 by storing only defect information. Third, precision stage optimization reduces travel time from 90 ms to 10 ms, boosting throughput by 2.75 times. The 9-beam system achieves 5.7 times higher throughput for physical defect detection, while the 25-beam system is projected to increase throughput by 10–13 times.[18] Core applications of this architecture include EUV mask verification (detecting pattern transfer defects with $> 99\%$ defect capture rate) and wafer voltage contrast (VC) inspection (identifying electrical defects like 7-nm FinFET gate leakage). In EUV mask inspection, MBSEM significantly reduces single-beam current density through parallel multi-beam architecture, fundamentally mitigating charge accumulation effects on insulating substrates and avoiding image distortion and inspection misjudgments caused by charging in traditional single-beam SEM. In voltage contrast inspection, parallel multi-beam acquisition extends single-beam dwell time under the same total beam current, significantly improving the signal-to-noise ratio and enabling reliable identification of weak electrical contrast defects (such as subsurface gate leakage paths). It can replace optical inspection for full-process quality control below 7-nm nodes. However, its design targets semiconductor scenarios, making it difficult to adapt to bioimaging's "large volume–low damage" requirements, resulting in limited versatility.

For a clear distinction of the three mainstream MBSEM architectures, a concise comparison based on unified engineering dimensions is as follows: The single-source single-column architecture has a beam count of $61 \sim 196$, with a hexagonal/square array and 25-μm pitch, per-beam current of 30 pA∼700 pA, typical landing energy of 10 keV∼20 keV (< 1 keV for low-damage imaging), and dominant detection modes of SE+TE; its main bottlenecks are beam count limited by ALA size and complex off-axis beam aberration correction, and it is mainly applied to large-volume biological tissue imaging and general material characterization. The split optical system architecture has a maximum beam count of 4, with a MEMS-fabricated array and 110-μm pitch, fixed landing energy of 12 keV, and high-purity SE detection; its main bottlenecks are limited throughput due to few beams and only medium-low resolution detection available, and it is dedicated to defect screening of 22-nm node semiconductor wafers. The semiconductor-specific MBI architecture has a beam count of $9 \sim 25$, with a $3 \times 3/5 \times 5$ high-density array, landing energy of 8 keV∼15 keV, and detection modes of SE+VC; its main bottlenecks are increased crosstalk risk with higher beam density and huge PB-scale data processing pressure, and it is the core tool for full-process inspection of 7 nm and below node wafers and EUV masks.

3. Key technological breakthroughs in MBSEM: from component optimization to system integration

The performance enhancement of MBSEM relies on the synergistic innovation across its three core modules: beam generation, imaging detection, and data processing. Recent technological breakthroughs in each module have not only resolved critical bottlenecks in multi-beam parallel processing but also propelled the system from laboratory prototypes to industrial practicality. These advancements represent not isolated component improvements, but rather cross-module technological coordination centered on the overarching objectives of enhancing beam uniformity (the relative deviation percentage of the current density and probe size of each sub-beam in the multi-beam array from the central beam, with a smaller deviation value indicating better uniformity), boosting signal sensitivity, and accelerating data processing.

3.1. Beam generation: from "quantity enhancement" to "uniformity control"

The "number" and "beam uniformity (the relative deviation percentage of the current density and probe size of each sub-beam in the multi-beam array from the central beam, with a smaller deviation value indicating better uniformity) "uniformity" of beam arrays form the foundation for determining MBSEM throughput and imaging quality. Early research focused on increasing the beam count, while recent efforts have shifted toward optimizing uniformity. Resolution variations caused by off-axis beam aberrations, such as field curvature and coma, have emerged as the core bottleneck constraining the performance of hundred-beam systems.

In electron source selection, Schottky field emission sources have become the mainstream choice due to their high brightness, low energy dispersion, and long-term stability. Both Delft and Zeiss systems employ ZrO/W Schottky sources, achieving brightness levels of 5×10^7 A/(m^2·sr·V). This enables support for 100 beams while maintaining single-beam currents between 30 pA and 700 pA (Zeiss 61-beam system: 570 pA per beam, total current 35 nA). Energy dispersion is only 0.5 eV FW50, minimizing chromatic aberration effects on multi-beam imaging; continuous operation for one year shows current fluctuation $< 1\%$, ensuring long-term imaging stability. Cold field emission (CFE) sources, while offering

higher brightness (5×10^8 A/(m^2·sr·V), 10 times that of Schottky sources) and supporting 500+ beam arrays, currently suffer from poor stability (current fluctuation $> 5\%$/hour). This requires improvements through source array packaging technology and has not yet been commercialized.

ALA's aberration correction technology is key to uniformity control. To address off-axis beam field curvature, the Delft system adjusts the voltage of ALA electrodes E1/E2 to slightly increase the focal length of the off-axis aperture lens beyond that of the on-axis lens, compensating for field curvature aberrations. After correction, the off-axis beam focal plane coincides with the on-axis plane, reducing the aberration contribution from 1.0 nm to 0.4 nm. Zeiss employs an asymmetric ALA design: the hexagonal ALA in the 61-beam system features edge apertures (19 μm) slightly larger than the central aperture (18 μm), balancing current density in off-axis beams to achieve full-field current uniformity fluctuations $< 5\%$. Furthermore, the application of MEMS processes further enhances ALA precision. Hitachi's MEMS–ALA achieves aperture position deviation < 100 nm, ensuring multi-beam parallelism. This provides manufacturing-level assurance for the beam uniformity. As shown in Fig. 2(a),[22] the validation image of a 91-beam SEM used for semiconductor inspection clearly demonstrates the device's high throughput, high resolution, and beam consistency in imaging semiconductor samples. This confirms that the MBSEM maintains nanometer-level fine resolution even in the high-throughput mode.

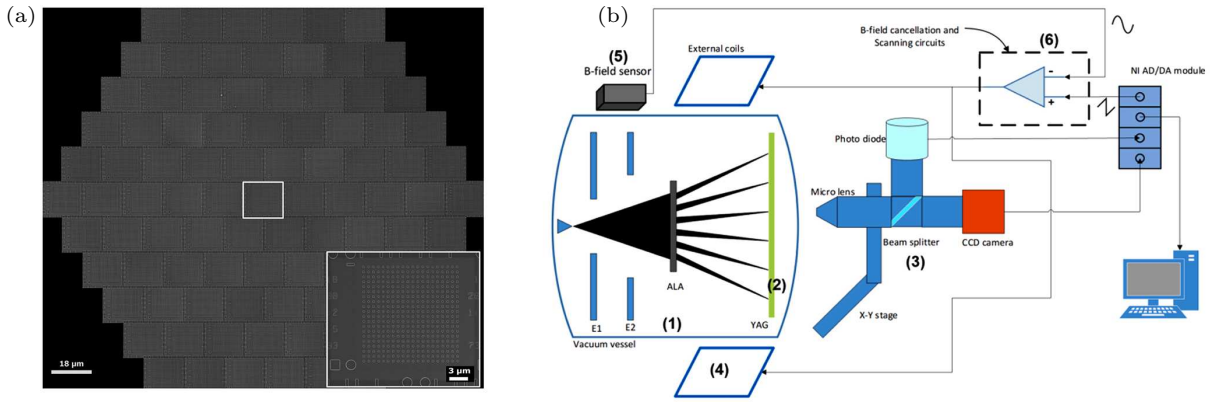


Fig. 2. Multi-beam source technology collaboration. (a) Verification image from a 91-beam SEM for semiconductor inspection, visually demonstrating the device's high throughput, high resolution, and beam coherence in imaging semiconductor samples,[21] reproduced with permission from Ref. [21]; (b) Schematic diagram of an experimental setup for measuring spot size and quadruple aberration effects in a multi-beam source (MBS),[22] reproduced with permission from Ref. [21].

3.2. Imaging detection: sensitivity and crosstalk control in SE/TE dual-mode detection

MBSEM must simultaneously achieve SE imaging (surface topography) and TE imaging (internal structure). The sensitivity and crosstalk (the percentage of the interference signal intensity relative to the target signal intensity when the detection signal of a single beam in the multi-beam array interferes with the detection channel of adjacent beams) control of these two detection systems directly determines imaging quality. Traditional SE detection relies on PMTs, which are bulky, power-hungry, and unsuitable for multi-beam parallel scenarios. In recent years, CMOS photodetectors coupled with YAG-fiber solutions have become mainstream. TE detection, tailored for thin biological tissues, achieves high-sensitivity and low-damage imaging through vacuum-integrated optics synchronized with high-speed cameras. The core breakthrough in SE detection lies in "miniaturization and low noise." The 0.35-μm CMOS photodetector developed by the Cambridge University team integrates a 100-μm ×100-μm NWD photodiode (response 0.33 A/W@850 nm), a low-noise transimpedance amplifier (TIA), and a select-merge circuit (SC): The TIA employs a three-stage push-pull inverting amplifier with feedback resistors implemented by PMOS transistors (lower noise than NMOS), achieving a transimpedance gain of 120 dB·Ω; The SC circuit uses PMOS switches to select and sum outputs from multiple TIA channels, with a linear summing range of 1.0 V–2.15 V. The chip achieves a total amplification of 180 dB·Ω, enabling detection of 1-nW low-power light. This replaces PMTs for miniaturization (chip size: 1960 μm×1960 μm). The Delft system employs a YAG-fiber-coupled scheme. A 30 μm thick YAG crystal converts SE into photons (conversion efficiency 21 photons/keV), with vacuum extraction via fiber-optic imaging catheters. Combined with 40× optical microscope magnification, SE signal crosstalk $< 2\%$, making it suitable for 196-beam high-density array detection. Optimized focusing for TE detection: "biological thin tissue adaptation." For imaging 30 nm–100 nm thin tissues in neuroscience, the Delft system places the sample directly on the YAG crystal. TE excitation of YAG luminescence is focused through a vacuum-sealed 40× objective (NA 0.95) to the camera, achieving 10 nm–20 nm detail resolution (e.g., mitochondria and endoplasmic reticulum in rat pancreatic tissue). Simultaneous acquisition of 196 TE beams completes imaging in < 1 hour. The Zeiss 61-beam system employs a camera with

1.2-GHz total bandwidth, completing imaging of a 3-mm^2 mouse brain slice (4-nm pixel size) in 20 minutes. The 290-GB dataset utilizes automatic alignment algorithms to achieve < 5 nm misalignment between slices, enabling subsequent 3D brain tissue reconstruction. Signal crosstalk control remains a common challenge in multi-beam detection. Current mainstream solutions include physical separation (e.g., magnetic beam separators, Wien filters) and electric field optimization (e.g., accelerating field compression aberration). ASML's 9-beam MBI system achieves crosstalk control of $< 2\%$ through optimized detector array spacing. However, as beam density increases (e.g., 500+ beams), pixelated direct electron detectors (with 90% efficiency) must be developed to further reduce crosstalk. Figure 2(b) shows a schematic of an experimental setup for measuring spot size and quadruple aberration effects in a multi-beam source (MBS).[23]

3.3. Data processing: real-time management and analysis of petabyte-scale data

MBSEM's high-throughput generates massive amounts of data — Zeiss's 61-beam system reaches 1 TB/hour, while the 196-beam system achieves 10 TB/hour. Traditional data processing architectures struggle to meet the demands of "real-time acquisition-compression-analysis." In recent years, distributed storage and AI-assisted analysis have emerged as breakthrough directions. The distributed storage architecture employs a layered design of "local caching + cloud storage": local caching uses NVMe SSDs (write speeds > 2 GB/s) to meet real-time acquisition demands and prevent data loss; the cloud stores PB-level data via distributed file systems (e.g., Ceph) to reduce data transfer latency. During idle periods, local data is synchronized to the cloud to ensure storage scalability. Data compression strategies are optimized for specific applications: bioimaging employs contour-based vector compression, achieving compression ratios of 10^2–10^3 (e.g., neural structures store only synapse and axon contours); semiconductor inspection employs die-to-database matching to store only defect information (location, size, type), achieving compression ratios $> 10^6$ and significantly reducing storage pressure. The integration of AI technologies further enhances data processing efficiency. Convolutional neural networks (CNNs) are widely used for real-time defect identification and neuronal structure segmentation, processing at 50 Gbps and reducing manual intervention; AI algorithms based on optical flow achieve sub-pixel alignment across multi-beam fields of view, reducing error to < 1 nm — significantly outperforming traditional mechanical correction (error > 5 nm); future real-time segmentation of petabyte-scale data using Transformer-based models is projected to increase processing speed by 10-fold, laying the foundation for real-time applications in hundred-beam systems.

4. Primary application areas of MBSEM

Multi-beam scanning electron microscope (MBSEM) breaks through the inherent trade-off between throughput and resolution of traditional single-beam SEM via a parallel electron beam imaging architecture. Relying on high imaging efficiency, nanoscale spatial resolution and flexible detection configuration, it has achieved large-scale applications in multiple key fields such as semiconductor manufacturing, neuroscience and geology. The core value of MBSEM is to obtain high-fidelity microstructural data at an efficiency much higher than that of conventional technologies, and to accommodate the sample properties and characterization needs across various fields. Based on relevant research findings, the following content systematically elaborates on the core application scenarios, technical advantages and scientific contributions of MBSEM.

4.1. Advanced process inspection in semiconductor manufacturing

As semiconductor technology advances toward N10, N7, and more advanced nodes, there is a continuous reduction in pattern size (with the minimum half-pitch as low as 24 nm), leading to exponential growth in requirements for defect detection sensitivity, critical dimension (CD) measurement accuracy, and inspection throughput.[24] Traditional single-beam SEM is limited by the trade-off between detector bandwidth and electron beam current, making it difficult to simultaneously meet the requirements of high resolution and large-scale inspection. The parallel imaging design of MBSEM has thus become the core technology to address this bottleneck.

As a representative commercial MBSEM device, the ZEISS multi-SEM has been successfully applied to process window characterization of the IMEC N10 logic node. As shown in Fig. 3(a), the Neumann group achieved stable imaging of TiN-etched logic M1 layout patterns by systematically optimizing pixel size (2 nm/4 nm) and scanning speed parameters. It can accurately track pattern variations caused by changes in the focus and dose of the lithography scanner and consistently capture systematic defects limiting the process window, such as bridging defects and line breaks. Experimental results indicate that the CD repeatability of the system can reach 0.64 nm at a 2-nm pixel size. Even at a 4-nm pixel size, it remains capable of reliably recognizing key defects, offering a high-efficiency solution for process closed-loop control of advanced-node semiconductors. Compared with the traditional single-beam SEM, the parallel scanning architecture of MBSEM reduces the inspection time of a single wafer by more than 60%, enabling full-wafer inspection in large-scale mass production. This conclusion is also supported by the research data of Ma and Eric's team in 2020.[18]

As semiconductor processes advance into 7 nm and below nodes (e.g., 5 nm, 3 nm), 3D stacked structures based on EUV

lithography (such as FinFET, GAA FET) pose dual challenges for defect inspection: first, defect sizes shrink to below 5 nm, requiring imaging resolution to surpass traditional limits; second, signal interference from multi-layer structures leads to a significant reduction in defect contrast.[12] To address this issue, Ma *et al.* proposed an MBSEM full-process inspection scheme in their 2019 study, achieving efficient and accurate detection through three key technological innovations, as shown in Fig. 3(b). First, it adopts a 128-beam parallel architecture and adaptive beam current distribution technology: high-current beams (50 pA per beam) are activated in core regions (e.g., gate trenches) to ensure resolution, while beam current is reduced in non-core regions to improve speed. Second, a multi-signal fusion detection module is developed to synchronously collect secondary electron (SE), backscattered electron (BSE), and energy-loss electron signals, distinguishing process defects from structural noise via machine learning algorithms. Third, a wafer-level coordinate calibration system is integrated to achieve precise matching of defect positions across processes from lithography, etching, to metallization, forming a full-process defect traceability link. Validation results of the solution in a 5-nm logic chip manufacturing line demonstrate that the capture rate for critical defects (e.g., excessive gate sidewall roughness, micro-shorts in metal interconnections) surpasses 92%. Moreover, the inspection time per process is kept within 8 minutes, representing an over 3-fold improvement compared to single-beam SEM, and addressing the dual challenges of "inspection bottleneck" and "cost burden" in advanced technology nodes. The Liebel group developed silicon drift detectors (SDD) based on a chip-level preamplifier design. This detector minimizes signal capacitance and parasitic capacitance, achieving a signal rise time of 40 ns and supporting artifact-free imaging with a pixel dwell time of 25 ns. Its gain-bandwidth product (GBWP) is an order of magnitude higher than that of conventional detectors.[24] The integration of this high-sensitivity and high-speed detector not only solves the spatial limitation of multi-signal parallel detection in multi-beam SEM but also optimizes the weak signal acquisition quality in low-dose imaging scenarios, providing key support for the refined inspection of advanced-node semiconductors (e.g., low-damage imaging, weak-contrast defect identification).[25]

Furthermore, the advancement of MEMS-based multi-beam optical systems has further extended the application scope of MBSEM for semiconductor characterization. The Ichimura group designed a 14×14 array microlens system, which can focus 196 electron beams onto a single point. It aims to achieve imaging performance with a total current of 200 nA and a resolution of 50 nm, suitable for material-level process optimization scenarios such as semiconductor thin-film thickness measurement and doping profile characterization.[13] Although this system faces the engineering challenge of high beam alignment complexity, experiments have confirmed the feasibility of MBSEM in high-current imaging applications. This finding also provides new ideas for the multi-dimensional characterization of semiconductor materials, which is supported by the subsequent research of the Doi team.[25]

For sub-3-nm nodes and the emerging "angstrom era" in semiconductor manufacturing, MBSEM technology continues to evolve. Lesire[26] *et al.* demonstrated at the 2024 European Mask and Lithography Conference the combination of massive e-beam inspection with CD-SEM contour analysis, achieving comprehensive analysis of process variability (including intra-wafer and intra-field components) through wafer-level dense measurements targeting poly contact short risks. These recent advances indicate that MBSEM technology is progressing toward higher resolution, higher throughput, and greater intelligence, directly addressing the challenges identified in the conclusion — "high-density beam arrays," "sub-nanometer resolution," and "real-time processing of PB-scale data" — providing critical technological support for full-process inspection at sub-3-nm nodes.

4.2. The large-volume imaging in neuroscience and biomedicine

Complete reconstruction of neural circuits (connectomics) demands nanoscale-resolution three-dimensional (3D) imaging of large-volume biological tissues. Traditional technologies like serial sectioning TEM are unable to fulfill whole-brain-scale imaging missions owing to their extremely low throughput.[9] Briggman and Bock pointed out in their review of volume EM technologies that, relying on high throughput and large field-of-view imaging capabilities, MBSEM has become one of the core technologies in connectomics research, promoting the leap of neuroscience from local circuit analysis to whole-brain connectome mapping. In the reconstruction of Drosophila brain neural circuits, the combination of ATUM (Automated Tape-collecting Ultramicrotome) technology and MBSEM exhibits significant advantages.[29] As shown in Fig. 3(c), the WaferMapper software developed by the Hayworth team works synergistically with the ATUM-SEM system. It can automatically map the spatial positions of thousands of 30 nm-thick ultrathin sections and rapidly acquire 3D EM datasets (1 TB–100 TB) of tissues such as mouse cerebellum and Drosophila brain via the multi-scale strategy of "low-resolution overview mapping and high-resolution targeted imaging".[27] The system leverages the parallel scanning capability of MBSEM to reduce the imaging time of a single section to the minute scale, achieving an imaging efficiency more than 40 times higher than that of conventional TEM.[31] Combined with in situ staining techniques such as ROTO developed by the Tapia team, MBSEM imaging can clearly display subcellular structures including neuronal mem-

branes, synaptic vesicles, and mitochondria, providing high-quality data support for neurite tracing and synaptic connection identification.

The construction of the whole-brain EM imaging dataset of adult Drosophila has further verified the application potential of MBSEM.[31] While Zheng *et al.* primarily employed TEMCA technology in their research, they explicitly indicated that multi-beam systems (e.g., ZEISS Multi-SEM) can further enhance throughput for future large-volume neural tissue imaging. The parallel imaging configuration effectively lowers the time overhead of large field-of-view mosaicking while retaining synaptic-level resolution at a 4-nm pixel dimension. Briggman and Bock also emphasized in their research that MBSEM (including multi-beam derivative technologies of SBFSEM and FIB-SEM) has become one of the three core technologies for neural circuit reconstruction. In the imaging of tissues such as zebrafish retina and mouse visual cortex, it can achieve 3D reconstruction of hundreds of cubic micrometers, revealing the connection specificity of direction-selective circuits.

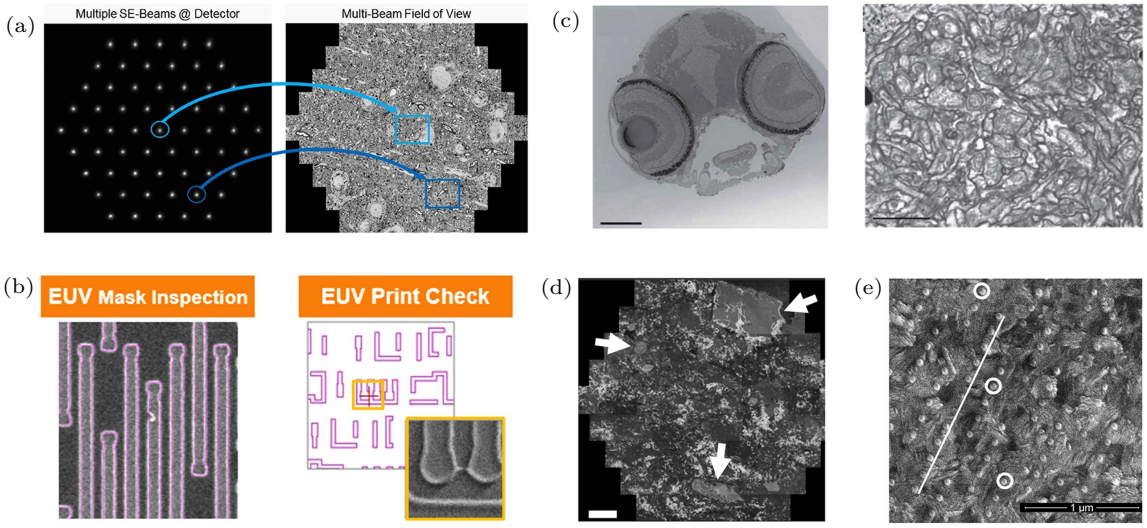


Fig. 3. Applications of MB-SEM in various fields. (a) Multi-beam SEM principle of operation,[24] reproduced with permission from Ref. [23]; (b) MBI Application for EUV mask and wafer,[12] reproduced with permission from Ref. [12]; (c) FESEM images of adult Drosophila brain ultrathin section mounted on Kapton tape,[27] reproduced with permission from Ref. [24]; (d) Image example taken on ZEISS multi-SEM 505,[28] Reproduced with permission from Ref. [28]; (e) single-beam SEM image of five successive 15-s exposures in the multibeam SEM at 15 keV,[26] reproduced with permission from Ref. [27].

The application of MBSEM in biomedicine has also extended to whole-brain-scale pathological research. Combined with the WB-PATCO whole-brain staining technology developed by Mikula *et al.*, MBSEM can uniformly characterize myelinated axons across the entire mouse brain, clearly track their distribution characteristics in gray and white matter, and provide a large-volume imaging tool for the study of pathological mechanisms of neurodegenerative diseases such as multiple sclerosis. In addition, studies by the Liebel team have confirmed that the low-dose imaging capability of MBSEM can reduce damage to biological samples caused by electron beams, protect the integrity of subcellular structures, and lay the foundation for high-resolution imaging of living-related samples.[24]

4.3. Characterization in geology and materials science

In geological research, the pore-space distribution and heterogeneity of mineral composition in unconventional oil and gas reservoirs such as shale are key factors affecting oil and gas recovery efficiency. Conventional single-beam SEM is unable to comprehensively characterize nanoscale pores in centimeter-scale samples owing to its restricted imaging scope. Meanwhile, the high throughput and large field-of-view imaging performance of MBSEM offers an innovative approach for the sophisticated characterization of shale.

Eberle *et al.* first applied ZEISS MultiSEM to the imaging of high-maturity shale rocks. Combined with broad ion beam polishing technology, they achieved full-coverage imaging with nanoscale resolution for centimeter-scale samples.[28] As shown in Fig. 3(d), MBSEM can clearly distinguish different mineral phases such as clay minerals and quartz, as well as tens-of-nanometer-scale pores. Its imaging results are highly consistent with the EDX elemental analysis data of single-beam SEM. Compared with the random sampling imaging of traditional single-beam SEM, MBSEM can acquire pore distribution data of the entire sample within hours, providing more comprehensive microstructural information for pore connectivity analysis and reservoir permeability prediction. This application has expanded the application boundary of MBSEM in non-biological fields.

MBSEM demonstrates extensive applicability in other areas of materials science as well. For instance, in the characterization of metal nanostructures, studies by the Ichimura team have confirmed that MBSEM's high-current imaging capability enables statistical measurement of grain size. By parallelly detecting the morphological characteristics of multiple grains,

it improves the reliability of analysis results; In polymer composite research, Ma Eric *et al*. indicated that MBSEM is capable of quickly imaging large-scale samples, distinctly revealing the distribution of fiber-reinforced phases and the status of interface bonding, thus offering data backing for the optimization of material properties.[18] Furthermore, Kruit *et al*. put forward that MBSEM's parallel electron beam-induced deposition (EBID) capability is applicable for the rapid prototyping of micro- and nano-devices. As shown in Fig. 3(e), multi-beam synchronous deposition greatly shortens the preparation time of complex structures.[26]

4.4. Emerging applications and technology convergence

In addition to the above core fields, MBSEM's applications have extended to various emerging contexts including micro- and nano-device fabrication and environmental science. In micro/nanodevice manufacturing, research by the Doi team has found that MBSEM's high-throughput imaging can be used for batch inspection of MEMS devices, rapidly identifying process defects such as photoresist residues and structural deformation, thus providing a guarantee for device yield improvement.[26] In environmental science, the Liebel team also pointed out that MBSEM can be used for the micromorphological characterization of atmospheric particulate matter and aquatic microplastics. Through parallel imaging, it rapidly analyzes the size distribution and surface characteristics of a large number of particles, providing technical support for research on pollutant source tracing and migration laws. In biomedicine, Team Zheng suggested that integrating MBSEM with correlative light and electron microscopy (CLEM) enables simultaneous acquisition of samples' fluorescence labeling information and high-resolution EM structural data. It achieves accurate correlation between specific protein localization and ultrastructure, offering a novel approach for investigating disease-related molecular mechanisms. In industrial inspection, research by Neumann *et al.* demonstrated that integrating MBSEM with machine learning algorithms enables automated defect detection and image segmentation, further enhancing the analysis efficiency of imaging data and facilitating the large-scale application of MBSEM in semiconductor and material manufacturing, as well as other fields. In basic science research, Briggman and Bock's study indicated that MBSEM is complementary to X-ray tomography. It can provide multi-dimensional structural characterization for biological tissues and material samples, supporting the resolution of cross-scale scientific problems.[32]

In summary, the applications of MBSEM have covered multiple key fields such as semiconductor manufacturing, neuroscience, and geology, with its core advantage lying in the simultaneous achievement of high throughput and high resolution. With the continuous advancement of detector technology, optical design, and data processing algorithms, the applications of MBSEM in scenarios such as advanced-process semiconductor inspection, whole-brain connectomics, and new material characterization will become more in-depth, providing strong imaging tool support for technological innovation and scientific discovery in various fields. In the future, the development of MBSEM will focus on higher beam number integration, lower-dose imaging, and more intelligent automated analysis, further expanding its application boundaries in cutting-edge scientific research and industrial production.

5. Conclusion and perspectives

Although MBSEM has achieved breakthrough applications in fields such as neuroscience, semiconductors, and biomedicine, its technological development still faces multi-dimensional bottlenecks, and these challenges are interrelated — beam uniformity directly affects imaging quality, signal crosstalk and detection efficiency restrict the scaling of multi-beam parallelism, and big data processing determines whether the high-throughput advantage can be fully exploited. The current core bottlenecks focus on three aspects: first, insufficient beam uniformity and aberration control. In hundred-beam systems, the resolution of edge beams is 20% lower than that of on-axis beams due to coma and field curvature (e.g., the Delft 196-beam system has an on-axis resolution of 1.2 nm and an off-axis resolution reduced to 1.48 nm). Additionally, under low landing energy (< 1 keV), the secondary electron (SE) signal intensity decreases by 50% and crosstalk increases to 5%–10%, which is difficult to meet the low-damage imaging requirements of biological samples; second, the balance challenge between signal crosstalk and detection efficiency. With the increase in beam density (spacing < 1 μm), the risk of SE signal overlap intensifies. The current optimal crosstalk control (e.g., $< 2\%$ in ASML 9-beam system) is difficult to adapt to the future demand for 500+ beams. In addition, transmission electron (TE) detection still relies on YAG crystals with a conversion efficiency of only 21 photons/keV, while direct electron detectors, although with an efficiency of 90%, cannot be compatible with multi-beam parallelism; third, the real-time bottleneck of big data processing. The data generation rate of hundred-beam systems reaches 10 TB/hour, and the existing 50-Gbps computing architecture is difficult to support real-time defect identification and image alignment. In addition, multi-beam field-of-view stitching relies on mechanical correction (error > 5 nm), and the sub-pixel level precision requirement has not yet been met.

To address the aforementioned challenges, the future development of MBSEM needs to focus on "breaking physical limitations and enhancing technological synergy" to form a multi-dimensional innovation path. First, high-density beam integration and resolution breakthroughs will be the core direction. 500+ beam integration will be achieved through cold field emission (CFE) arrays and MEMS aperture lens

arrays (ALA), combined with adaptive multipole correctors (6-pole/12-pole) to compensate for off-axis aberrations, aligning the resolution of edge beams with that of on-axis beams and advancing the implementation of sub-nanometer resolution. Meanwhile, optimize the low-energy SE extraction electric field (e.g., electrostatic–magnetic composite field) to alleviate signal attenuation and crosstalk in low-dose imaging. Second, multi-modal fusion and detection efficiency upgrading will enhance system versatility. Integrate CMOS photon detectors and multi-channel direct electron detectors to simultaneously acquire sample surface topology (SE), internal structure (TE), and electrical characteristics (VC), which not only solves the problem of low TE detection efficiency but also meets the requirements for semiconductor "structure–function" collaborative detection and neuron "morphology–function" correlation analysis. Third, AI technology will empower the entire process. On one hand, real-time optimization of ALA voltage and objective lens parameters will compensate for beam drift; on the other hand, the Transformer model will be used to increase the real-time segmentation and defect identification speed of PB-scale data (expected to increase by 10 times). Meanwhile, the optical flow method will be combined to reduce the multi-beam field-of-view alignment error to < 1 nm, solving the problem of insufficient mechanical correction accuracy. Finally, cross-scale and cross-modal correlation will expand the application boundaries of MBSEM. Through collaboration with optical microscopes (confocal, super-resolution), a research link of "macroscopic positioning (optical)–microscopic imaging (MBSEM)" will be constructed, which not only solves the cross-scale analysis problem of "whole brain–single cell" in neuroscience but also meets the demand for full-process monitoring of "wafer–chip" in semiconductors, promoting MBSEM from a single imaging tool to a core platform connecting microstructures and macroscopic functions.

Acknowledgements

Project supported by the National Key Research and Development Program of China (Grant Nos. 2021YFA1200600, 2024YFA1208902, and 2024YFA1408000), the National Natural Science Foundation of China (Grant Nos. 52231007, 12327804, T2321003, 22088101, and 22405050), the Science and Technology Commission of Shanghai Municipality (Grant No. 24ZR1406400), and Shanghai Municipal Education Commission (Grant No. 24KXZNA06).

References

[1] Huang Y, Zhao Y, Bai W, Cao Y, Xu W, Shen X and Wang Z 2024 *Process Safety and Environmental Protection* **191** 1483
[2] Dong C, Wei L, Zhu W, Kim J K, Wang Y, Omotara P, Arsana A and Wang B Z 2025 *ACS Nano* **19** 25526
[3] Huang Y, Chen T, Ren C, Bao B, Huang R, Sun Y, Yu C, Yang Y, Wong W T, Zeng Q, Jiang L, Liu T, Lin Q, Zhu L and Liao Y 2025 *Adv. Mater.* **37** 2501051
[4] Zhao L, Feng M, Wu C, Guo L, Chen Z, Risal S, Ai Q, Lou J, Fan Z, Qi Y and Yao Y 2025 *Nat. Commun.* **16** 4283
[5] He X, Gong G, Chen M, Zhang H, Zhang Y, Richardson J J, Chan W Y, He Y and Guo J 2024 *Angewandte Chemie International Edition* **63** e202314501
[6] Robinson A W, Wells J, Moshtaghpour A, Nicholls D, Huang C, Velazco-Torrejon A, Nicotra G, Kirkland A I and Browning N D 2024 *Chin. Phys. B* **33** 116804
[7] Nellist P D and Pennycook T J 2024 *Chin. Phys. B* **33** 116803
[8] Lei Yihan Y, Song Jiahao, Ge Jinxin, Wu Dirui, Zhang Yingli, Li Changjian 2024 *Chin. Phys. B* **33** 096801
[9] Briggman K L and Bock D D 2012 *Curr. Opin. Neurobiol.* **22** 154
[10] Eberle A L and Zeidler D 2018 *Front. Neuroanat.* **12** 112
[11] Horstmann H, Korber C, Satzler K, Aydin D and Kuner T 2012 *PLoS One* **7** e35172
[12] Ma E L, Chou K, Ebert M, Liu X, Ren W, Hu X, Maassen M, Yin W, Chen A, Wang F, Patterson O D, Adan O and Ukraintsev V A 2019 *SPIE* **10959** 109591
[13] Ichimura T, Ren Y and Kruit P 2014 *Microelectronic Engineering* **113** 109
[14] Lichtman J W and Denk W 2011 *Science* **334** 618
[15] Mohammadi-Gheidari A, Hagen C W and Kruit P 2010 *Journal of Vacuum Science & Technology B* **28** C6G5
[16] Micheva K D and Smith S J 2007 *Neuron* **55** 25
[17] Eberle A L, Mikula S, Schalek R, Lichtman J, Tate M L K and Zeidler D 2015 *J. Microsc.* **259** 114
[18] Ma E L, Ren W, Luo X, Zhao S, Hu X, Liu X, Kuan C, Chou K, Maassen M, Yin W, Chen A, Sen N, Ebert M, Liu L, Wang F, Patterson O D, Adan O and Robinson J C 2020 *SPIE* **11325** 113250
[19] Mohammadi-Gheidari A and Kruit P 2011 *Nuclear Instruments and Methods in Physics Research Section A* **645** 60
[20] Enyama M, Sakakibara M, Tanimoto S and Ohta H 2014 *Journal of Vacuum Science & Technology B* **32** 051801
[21] Cain J P, Sanchez M I, Kemen T, Malloy M, Thiel B, Mikula S, Denk W, Dellemann G and Zeidler D 2015 *SPIE* **9424** 119
[22] Mohammadi-Gheidari A, Kieft E R, Guo X, Wisse M and Kruit P 2023 *Ultramicroscopy* **249** 113735
[23] Sanchez M I, Ukraintsev V A, Neumann J T, Garbowski T, Högele W, Korb T, Halder S, Leray P, Garreis R, le Maire M and Zeidler D 2017 *SPIE* **10145** 2115
[24] Liebel A, Lutz G, Weber U, Schmid M, Niculae A and Soltau H 2016 *Microscopy and Microanalysis* **22** 598
[25] Doi T, Yamazaki M, Ichimura T, Ren Y and Kruit P 2016 *Microelectronic Engineering* **159** 132
[26] Post P C, Mohammadi-Gheidari A, Hagen C W and Kruit P 2011 *Journal of Vacuum Science & Technology B* **29** 06F310
[27] Tapia J C, Kasthuri N, Hayworth K J, Schalek R, Lichtman J W, Smith S J and Buchanan J 2012 *Nat. Protoc.* **7** 193
[28] Lena Eberle A, Garbowski T, Bhattiprolu S, Crosby K and Zeidler D 2017 *Microscopy and Microanalysis* **23** 2114
[29] Hayworth K J, Morgan J L, Schalek R, Berger D R, Hildebrand D G and Lichtman J W 2014 *Front. Neural Circuits* **8** 68
[30] Hayworth K J, Kasthuri N, Schalek R and Lichtman J W 2006 *Microscopy and Microanalysis* **12** 86
[31] Zheng Z, Lauritzen J S, Perlman E, Robinson C G, Nichols M, Milkie D, Torrens O, Price J, Fisher C B, Sharifi N, Calle-Schuler S A, Kmecova L, Ali I J, Karsh B, Trautman E T, Bogovic J A, Hanslovsky P, Jefferis G, Kazhdan M, Khairy K, Saalfeld S, Fetter R D and Bock D D 2018 *Cell* **174** 730
[32] Chang H, Docheva D, Knothe U R and Knothe Tate M L 2014 *Stem. Cells Transl. Med.* **3** 308